Journal of Materials Chemistry A

Sharp-Tip Enhanced Catalytic CO Oxidation by Atomically Dispersed Pt1/Pt2 on Raised Graphene Oxide Platform

Journal:	*Journal of Materials Chemistry A*
Manuscript ID	TA-ART-04-2020-004156.R1
Article Type:	Paper
Date Submitted by the Author:	09-Jun-2020
Complete List of Authors:	Jia, Chuanyi; Guizhou Provincial Key Laboratory of Computational Nano-material Science, Guizhou Normal College Zhang, Yujin; School of Electronic and Information Engineering (Department of Physics), Qilu University of Technology Wang, Xijun; University of Science and Technology of China, Physical Chemistry Zhong, Wenhui; Guizhou Normal College, Key Laboratory of Computational Nano-Material Science Prezhdo, Oleg; University of Southern California, Chemistry Luo, Yi; University of Science and Technology of China, Hefei National Laboratory for Physical Sciences at the Microscale Jiang, Jun; University of Science and Technology of China , School of Chemistry and Materials Science

Sharp-Tip Enhanced Catalytic CO Oxidation by Atomically Dispersed Pt_1/Pt_2 on Raised Graphene Oxide Platform

Chuanyi Jia [a, b],‡ Yujin Zhang [c],‡ Xijun Wang [b],‡ Wenhui Zhong [a], Oleg V. Prezhdo [d], Yi Luo [b], Jun Jiang [b,*]

a) Guizhou Provincial Key Laboratory of Computational Nano-material Science, Institute of Applied Physics, Guizhou Education University, Guiyang, Guizhou, 550018, China

b) Hefei National Laboratory for Physical Sciences at the Microscale, iChEM (Collaborative Innovation Center of Chemistry for Energy Materials), CAS Center for Excellence in Nanoscience, School of Chemistry and Materials Science, University of Science and Technology of China, Hefei, Anhui, 230026, China

c) School of Electronic and Information Engineering (Department of Physics), Qilu University of Technology, Jinan, Shandong, 250353, China

d) Department of Chemistry, University of Southern California, Los Angeles, California, 90089, United States

‡ The first three authors contributed equally to this work.

ABSTRACT:

Revealing structure-activity relationships of graphene-supported atomically dispersed transition metal catalysts is of key importance in catalysis chemistry and materials science. Here we report a first-principles theoretical study on O_2 activation and CO oxidation catalyzed by atomically dispersed Pt_1/Pt_2 anchored on a raised graphene (Gr) platform. The unique sharp-tip structure of the protuberant graphene platform (carbon-tip) can collect extra polarization electrons on the Pt-tip, promoting electron transfer between the catalyst and adsorbates, and greatly enhancing the chemical activity. Higher carbon-tips on defective graphene oxide with a carbon vacancy (Gr-V) produce more polarization electrons, a more localized electric field, and a larger up-shift of the d-orbital center of the Pt-tip, resulting in better catalytic performance. The carbon-tip enhancement reduces the energy barrier for the CO oxidation on Pt_1O_2/Gr-V from 1.19 eV to 0.56 eV compared with Pt_1 on planar Gr. In addition, CO poisoning is significantly alleviated, with the CO poisoning rate $\boldsymbol{\Gamma_o}$ reduced from 2.00 eV to 0.52 eV. Moreover, a linear relationship between the activation barrier and the binding energy of adsorbates is found for various atomically dispersed Pt-tip catalysts on the raised graphene oxide platform. Importantly, the order of catalytic activity is consistent with the carbon-tip enhancement, *i.e.*, Pt_1O_2/Gr-V > Pt_2O_4/Gr-V > Pt_1O_2/Gr > Pt_2O_4/Gr. These findings provide important guidance for rational design of atomically dispersed catalysts.

1. INTRODUCTION

Atomically dispersed metal catalysts are among the most promising types of heterogeneous catalysts in many reactions including automobile exhaust treatment,[1-5] oxygen reduction reaction,[6-8] hydrogen production,[9-11] and other processes.[12-15] They provide a promising way to minimize the use of expensive metals so as to fulfill the ultimate goal of cost-effective catalysis. Recently, dramatic developments have been made in creating efficient atomically dispersed transition metal (TM) catalysts, while the search for appropriate supports and control of TM anchoring morphology remain challenging.

Owing to many merits of low-cost, large surface area and high conductivity, graphene (Gr) based materials are good candidates to support atomically dispersed TM catalysts.[16-18] As a result, many works have investigated various structural factors of Gr-supported TMs that play important roles in deciding catalytic performance. For example, using the metal-organic framework assisted method, Ren et al.[19] found that isolated diatomic Ni-Fe sites anchored on nitrogenized graphene can generate an efficient electrocatalyst for CO_2 reduction. A study of the graphene composite materials with single Co active sites by Cui et al.[20] pointed out that the microstructure of the supported Co has a significant influence on the catalytic performance. A systematic study by Zhang et al.[21] revealed that the diverse support defects in graphene can induce different local density of states of atomic Ni species, substantially promoting the catalytic selectivity of Ni/Gr catalysts. Recent experimental and theoretical studies

conducted in our group have revealed that nanometer-sized tips of TM catalysts can induce strong local electric fields, which in turn strongly promote catalytic activity.[22,23] Consequently, we identified the nanometer-sized sharp-tip enhancement effect as a crucial issue for atomically dispersed TM catalysts, requiring deeper understanding in order to provide useful guidance for development of cost-effective catalytic materials.

Herein, the single/double-atom based Pt_1/Pt_2 TM catalysts anchored on a raised graphene oxide platform, newly synthesized and reported as potential catalysts for many reactions,[24] were systematically investigated by the density functional theory (DFT) calculations, to reveal the structure-activity relationship underlying the sharp-tip enhanced effect. The catalytic performances of the Pt-tip sites are characterized with the O_2 activation and CO oxidation reactions, which are widely recognized as essential for solving the energy and environmental crisis.[25,26] Microkinetics simulations demonstrate that the Pt_1O_2 tip on the defective graphene oxide support offers the strongest activity in the O_2 activation and CO oxidation. A high carbon-tip in Pt_1O_2/Gr-V can significantly reduce the energy barrier and alleviate the CO poisoning effect. Importantly, a linear relationship between the activation barrier and binding energy of adsorbates for various atomically dispersed Pt-sites on graphene was revealed. Since many catalytic reactions rely on a strong local electric-filed, the field distribution found in this work are strongly correlated to the extension of the carbon-tip on the support, providing key information for designing high-performance catalysts for various applications.

2. CALCULATION DETAILS

Spin-polarized DFT calculations were performed using the Vienna ab initio simulation package (VASP).[27] Geometric and electronic properties were simulated with the Perdew, Burke and Ernzerhof (PBE) functional and the projector augmented wave (PAW) method.[28-31] The empirical correction method (DFT-D2) was applied to describe the long-range van der Waals (vdW) interactions (the convergence test is shown in Supporting Information-Section 1).[32] For geometry optimization, the convergence criterion of total energy and force were set to 10^{-5} eV and 0.01 eV/Å, respectively. The Brillouin zone was sampled with 5 × 5 × 1 Monkhorst-Pack k-meshes, and the kinetic energy cutoff of 400 eV was used for the plane-wave expansion.[33,34] For the density of states (DOS) calculation, the k-point value was increased to 15 × 15 × 1 to achieve high accuracy.

The graphene monolayer was modeled using a hexagonal 6 × 6 supercell with 72 carbon atoms.[33,34] The vacuum region preventing spurious image interactions was set to 15 Å. The DDEC6 method which is a refinement of the Density Derived Electrostatic and Chemical (DDEC) approach was adopted to examine the charge transfer effect.[35,36] The reliability and accuracy of this method have been repeatedly verified by many theoretical and experimental works, showing that it has excellent performances in 2D/3D solid material systems.[37-39] The transition states of O_2 activation and CO oxidation reactions were searched by the climbing image nudged elastic band (CI-NEB)

method.[40,41] The detailed calculation steps for the reaction paths are shown in the Supporting Information-Section 2.

The binding energy between the adsorbate and catalyst surface is calculated as:

$$E_b = E_{sur+ad} - E_{sur} - E_{ad} \quad (1)$$

where E_{sur+ad}, E_{sur}, and E_{ad} denote the energies of the surface-adsorbate configuration, and isolated surface and molecule, respectively.

To quantitatively compare the CO poisoning effect on different supported Pt sites, we have imported a new descriptor CO poisoning rate Γ_θ, as given by:

$$\Gamma_\theta = kT \ln(\frac{\theta_{CO}}{\theta_{O_2}}) \quad (2)$$

Here, k is the Boltzmann constant; T is the temperature; $\frac{\theta_{CO}}{\theta_{O_2}}$ is the ratio between the coverage of CO and O_2 (details in the Section 3 of Supporting Information). According to this definition, a larger Γ_θ means stronger CO poisoning effect on the active site.

3. RESULTS AND DISCUSSION

3.1 O_2 Activation and CO Oxidation by Oxidized Pt_1 on Pristine Graphene Surface.

The oxidized Pt_1 single atoms and Pt_2 dimers on Gr are modeled using the Pt_1O_2/Gr and Pt_2O_4/Gr which have been confirmed as reasonable structures in experimental observations.[24] To examine the structural stability, various Pt_1O_2 binding sites including the Ortho, Meta, and Para positions over the carbon ring have been investigated (details in the Section 4 of Supporting Information). It is found that the Pt_1O_2 prefers to be

adsorbed at the Ortho-positioned carbon sites (Figure S3), which was then taken for subsequent calculations.

As a reference, the single-atom based Pt_1 supported by a pristine Gr was calculated, resulting in an optimized structure of Pt_1/Gr in Figure 1a. Here the protuberant Pt_1 acts like a nanometer-sized sharp-tip, collecting a few polarization electrons. Although the electronegativity of Pt (2.28)[42] is lower than that of C (2.55)[43], the Pt_1 still gains electrons of ~0.04 e from the support (the Pt_1 on Pt_1/Gr become 0.04 e negative charged). In contrast, the electronegativity of the interfacial O atoms (3.44)[43] in Pt_1O_2/Gr is much higher than that of C, causing a substantial number of electrons being transferred from support to the Pt_1O_2 cluster (the Pt_1O_2 cluster holds 0.37 e negative charge in total, as shown in Figure S4). Meantime, the Pt_1 atom also donates electrons to O atoms and itself become positively charged (the Pt_1 on Pt_1O_2/Gr holds -0.35 e positive charge), which in turn change the electric field around it. As depicted in Figure 1d, the electric field on the positively charged Pt_1 in Pt_1O_2/Gr is much stronger than that on the pure Pt_1/Gr system. This response can promote the adsorption of O_2 (normally negative charged) by enhancing the electrostatic attraction between adsorbate and Pt site.

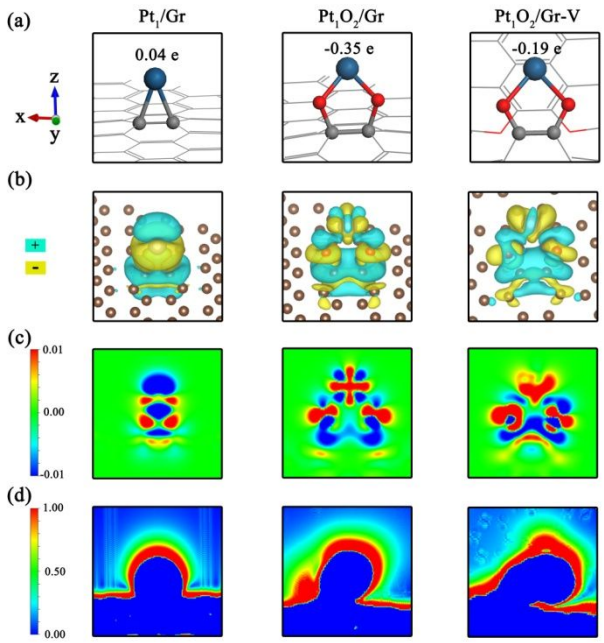

Figure 1. The optimized binding structures and corresponding electronic properties of the Pt_1/Gr, Pt_1O_2/Gr and Pt_1O_2/Gr-V configurations. (a) Binding structures and DDEC (density derived electrostatic and chemical) charges of Pt atoms; (b) three-dimensional (3D) differential charge density maps; (c) two-dimensional (2D) differential charge density maps; (d) 2D electric field maps (along the yz-plane). Dark blue, gray, and red spheres represent Pt, C, and O atoms, respectively.

As a starting point, the O_2 adsorption and activation on Pt_1/Gr and Pt_1O_2/Gr are calculated. As expected, the positively charged Pt atom with strong electric field in Pt_1O_2/Gr holds lower adsorption energy (-2.42 eV) for O_2 adsorption than that of Pt_1/Gr (-1.43 eV) (Figure S5). Meanwhile, the strong dependence of O_2 binding energies on the electronic structures of Pt sites has a profound impact on the kinetics of O_2

activation. As depicted in Figure 2a, the energy barrier for O_2 dissociation is reduced from 1.46 eV for Pt_1/Gr to 1.18 eV for Pt_1O_2/Gr.

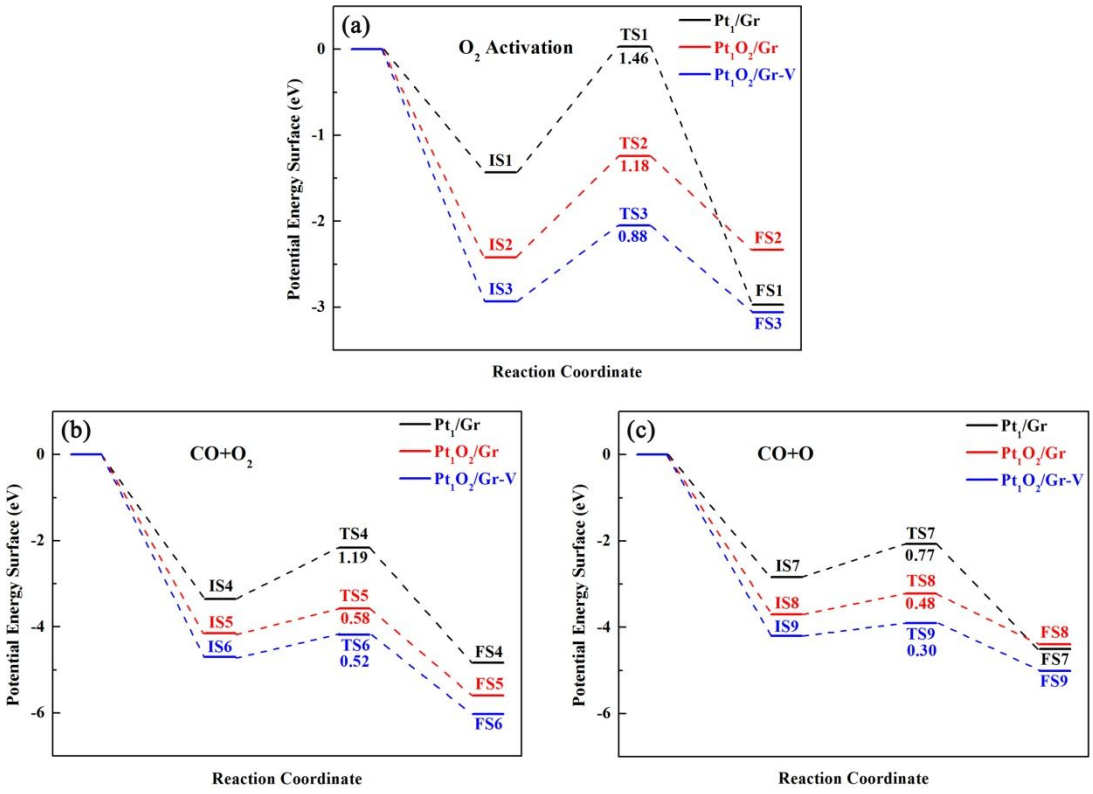

Figure 2. Potential energy diagrams for O_2 activation and CO oxidation (including the $CO+O_2$ and CO+O steps) on the Pt_1/Gr, Pt_1O_2/Gr and Pt_1O_2/Gr-V catalysts. The total energies of bare surface and free molecules are set to 0 eV. The optimized structures (including the transition states) and their binding energies are shown in Figures S6-S7.

It is well-accepted that the synergistic effect between the reactants usually plays important roles.[44-47] To reach a comprehensive understanding of graphene supported Pt catalysts, a further exploration of CO oxidation was carried out. The binding energies

of O_2 and CO in Table 1 (with binding structures in Figure S5 and S8) show that the strong electric field on the active Pt_1 site in Pt_1O_2/Gr can significantly promote the adsorption of O_2 (adsorption energy from -1.43 eV to -2.42 eV), and however has little influence in helping capture CO molecule (adsorption energy from -3.26 eV to -3.06 eV). As listed in Table 1, the approximation of the binding energies between CO and O_2 can reduce the value of CO poisoning rate Γ_o (from 2.00 eV to 0.80 eV), which further alleviates the CO poisoning effect on the active Pt site in Pt_1O_2/Gr.

Table 1. Calculated binding energies (E_b), energy difference (ΔE) and CO poisoning rate Γ_o of O_2 and CO on different Pt sites. $\Delta E = E_b(O_2) - E_b(CO)$

	$E_b(O_2)$ (eV)	$E_b(CO)$ (eV)	ΔE (eV)	Γ_o (eV)
Pt_1/Gr	-1.43	-3.26	1.83	**2.00**
Pt_1O_2/Gr	-2.42	-3.06	0.64	**0.80**
Pt_1O_2/Gr-V	-2.93	-3.28	0.35	**0.52**
Pt_2/Gr	-1.37	-2.80	1.43	**1.58**
Pt_2O_4/Gr	-2.16	-2.58	0.42	**0.59**
Pt_2O_4/Gr-V	-2.51	-2.88	0.37	**0.55**

For CO oxidation, single ($CO+O_2$) and multiple ($2CO+O_2$) CO reaction mechanisms have been tested. The calculation results indicate that because of the large repulsive force from the pre-adsorbed 2CO, the O_2 molecule cannot be stably adsorbed and is

more inclined to leave far away from the surface. It means that the multiple CO reaction mechanism ($2CO+O_2$) can hardly occur on the active Pt sites, as shown in Figure S9. Thus, we mainly analyzed the $CO+O_2$ reaction mechanism in this work. On Pt_1/Gr, the energy barrier of the "$CO + O_2 \rightarrow CO_2 + O$" step is 1.19 eV, being lower than that of the corresponding O_2 dissociation reaction (1.46 eV), as seen in Figure 2a and 2b. This improvement is ascribed to the synergistic effect between the co-adsorbed CO and O_2. When CO and O_2 react on Pt_1/Gr, a metal-stable four-center transition state (O-O-CO) is formed due to the strong interactions between the C (in CO) and O (in O_2) atoms (Figure S6), which promotes the structural stability of the transition state[44] (**TS4**) and thereby lower the energy barrier. Moreover, the strong electric field on the Pt-tip site in Pt_1O_2/Gr improves the stability of the initial binding state (**IS5**) and transition state (**TS5**) of the co-adsorbed CO and O_2 configuration as well. Thus, compared to Pt_1/Gr, the activation barrier for "$CO + O_2 \rightarrow CO_2 + O$" on Pt_1O_2/Gr is further reduced from 1.19 eV to 0.58 eV. For the second step of "$CO + O \rightarrow CO$", because the residual O atom on Pt is more active than O_2, the activation barrier of this step is lower than the first step, as shown in Figure 2c. As a result, the reaction between the co-adsorbed CO and O_2 is the rate-determining step for CO oxidation on Pt_1/Gr and Pt_1O_2/Gr. It should be emphasized that the electric field enhancement effect on the oxidized Pt site can also promote the CO + O reaction via enhancing the structural stability of **IS8** and **TS8** (Figure S7). Correspondingly, the activation barrier for this step is reduced from 0.77 eV for Pt_1/Gr to 0.48 eV for Pt_1O_2/Gr. These results demonstrate that the presence of

the interfacial O atoms in Pt_1O_2/Gr has a strong impact on the electronic structure of the supported Pt atom (especially the electric field), which can alleviate the CO poisoning effect and promote the O_2 activation and CO oxidation reactions on the catalyst surface.

3.2 O_2 Activation and CO Oxidation by Oxidized Pt_1 on Defective Graphene Surface.

It is interesting to note from Figure 3 that the strong interaction between Pt_1O_2 cluster and Gr support causes a raised Gr supporting platform (labeled as carbon-tip for the pulled up C atoms in Gr). In order to gain insight into this special structure, a defective Gr with one carbon vacancy to support the Pt_1O_2 catalyst is built for further investigation. Since the Pt_1 single atoms and Pt_2 dimers will be exposed to O_2 or O_3 environment during synthesis in experiment, the carbon vacancy should be covered by O atoms.[24] After testing two possible configurations (Ortho and Meta), replacing Ortho-positioned C atom with O atom is found to be stable upon Pt_1O_2 adsorption (Figure S10), which fits well with previous experimental results.[24] This model with oxidized carbon vacancy (labeled as Gr-V) is then used in the following studies of O_2 activation and CO oxidation.

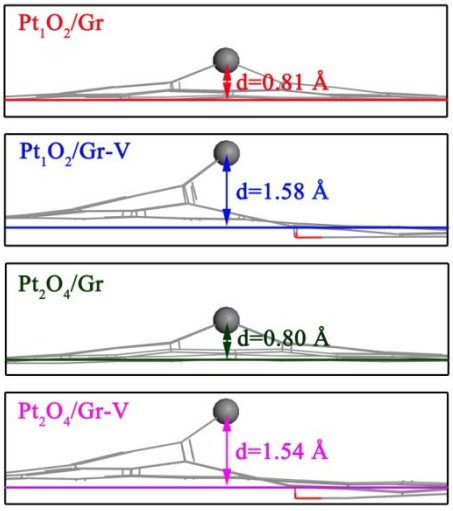

Figure 3. The structures of the carbon-tip on the Pt_1O_2/Gr, Pt_1O_2/Gr-V, Pt_2O_4/Gr and Pt_2O_4/Gr-V surfaces (for easy observation, the oxidized Pt atoms have been deleted). z is the ordinate of the carbon atom; d is the distance between the top of the carbon-tip and the average ordinate of the remaining atoms.

Our calculations show that the defective graphene oxide with carbon vacancies (Gr-V) can generate a higher carbon-tip than that on pristine Gr. As illustrated in Figure 3, the height of the protuberant C atoms is increased from 0.81 Å on pristine Gr to 1.58 Å in Pt_1O_2/Gr-V. This further promotes the collection of polarization electrons on the Pt-tip, increasing the electron transferring from support to Pt_1O_2 (0.45 e in Figure S4). The DDEC charge analysis in Table 2 confirms that when O_2, $CO+O_2$ and CO+O were adsorbed on Pt_1O_2/Gr-V, the Pt_1 atom can donate more electrons to the adsorbates than that on Pt_1O_2/Gr.

Table 2. The charge difference (before and after adsorption) of the active Pt sites **(Pt)** and the adsorbates **(ad)** on the Pt_1O_2/Gr and Pt_1O_2/Gr-V catalysts. $\Delta q = q_{aft} - q_{bef}$

	$\Delta q(O_2)$ (e)	$\Delta q(CO+O_2)$ (e)	$\Delta q(CO+O)$ (e)
Pt_1O_2/Gr(Pt)	-0.14	-0.07	-0.24
Pt_1O_2/Gr(ad)	0.30	0.21	0.32
Pt_1O_2/Gr-V(Pt)	-0.19	-0.18	-0.35
Pt_1O_2/Gr-	0.32	0.26	0.44

The electron transferring in Pt_1O_2/Gr-V further changes the electronic structure of Pt_1. It is clearly shown from three- and two-dimensional (3D and 2D) differential charge density maps in Figure 1b and 1c that positive charges are mainly located on the top of Pt_1 in Pt_1O_2/Gr-V. As a result, Figure 1d indicates that the electric fields on Pt_1 in Pt_1O_2/Gr-V become more concentrated and mainly locates on the top site (the main binding site for the adsorbates). Such localized electric fields on Pt_1O_2/Gr-V will be more powerful in attracting negatively charged adsorbates in comparing with the decentralized electric field in Pt_1O_2/Gr.

Besides the distribution of the surface electric field, the d-orbital center for the electronic states of TMs also play important roles.[48] From the partial density of state (pDOS) in Figure 4, one can see that the d-orbital center of the Pt_1 atom in Pt_1O_2/Gr-V has a significant up-shift in regarding to the Fermi level (from -2.43 eV to -1.30 eV).

The up-shift of d-orbital states can push the anti-bonding states above the Fermi level and decrease the Pauli repulsion,[48] which further increases the bond strength between adsorbates and TMs.

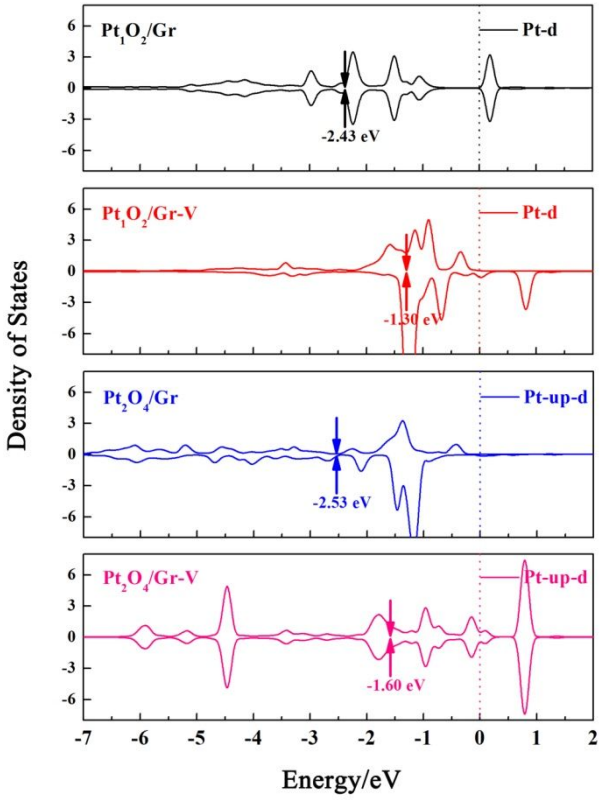

Figure 4. Projected d-orbital on the partial density of states (pDOS) of the Pt-tip atoms on the Pt_1O_2/Gr, Pt_1O_2/Gr-V, Pt_2O_4/Gr and Pt_2O_4/Gr-V surfaces. The d-orbital center is marked by the double arrows. The Fermi level is set to 0 eV.

With the results above, the impacts of the high carbon-tip on Gr-V can be concluded as follows: (i) inducing polarization electrons on the active Pt_1 site; (ii) making the electric field more localized on the Pt_1-tip; and (iii) up-shifting the d-orbital center of Pt_1 toward the Fermi level. These three responses not only enhance the interactions

between the adsorbates and catalysts, but also promote activities.

The underlying kinetics of catalytic reactions was then examined. The potential energy diagram for O_2 activation (Figure 2a) shows that the high carbon-tip on Gr-V can achieve high structural stability for O_2 adsorption (-2.93 eV adsorption energy in Figure S5) and low reaction energy barrier of 0.88 eV. Similar to Pt_1O_2/Gr, the change of electronic structures on Pt_1 in Pt_1O_2/Gr-V has little influence on the structural stability for CO adsorption (from -3.06 eV to -3.28 eV). Thus, compared to Pt_1O_2/Gr, the value of CO poisoning rate $\boldsymbol{\Gamma_o}$ on Pt_1O_2/Gr-V is further reduced from 0.80 eV to 0.52 eV. This means that under typical reaction conditions, reactants of CO and O_2 will hold greater opportunities to be co-adsorbed on the Pt_1O_2/Gr-V surface than Pt_1O_2/Gr, resulting in higher catalytic performance. For CO oxidation, because of the stronger sharp-tip enhancement effect, the stabilities of co-adsorbed CO+O_2 (from -4.15 eV in Pt_1O_2/Gr to -4.70 eV) and CO+O (from -3.70 eV in Pt_1O_2/Gr to -4.20 eV) on Pt_1O_2/Gr-V are significantly improved (Figure S6 and S7). These improvements further lower the reaction energy barriers from 0.58 eV to 0.52 eV, and 0.48 eV to 0.30 eV, respectively. Therefore, compared to the pristine graphene support, the Pt_1O_2 on the defective graphene oxide with carbon vacancy is more efficient for O_2 activation and CO oxidation.

3.3 O_2 Activation and CO Oxidation by Oxidized Pt_2 on Pristine Graphene Surface.

Besides introducing carbon defects, increasing the number of atomic layers below the Pt-tip may provide another knob to engineer the atomic structure, charge distribution, and d-orbital of the graphene supported TMs. To identify the most feasible four-layered oxidized Pt_2 on graphene, the Pt_2O_4 on the Ortho, Meta, and Para positions of the carbon ring on Gr have been tested (Figure S11). It was found that the Ortho-positioned binding state of Pt_2O_4/Gr with the structure similar to Pt_1O_2/Gr is energetically more favorable to occur. In contrast to the Pt_2O_4 on Gr, the referenced system of Pt_2 on pristine Gr (Pt_2/Gr) is inclined to be adsorbed on the top of one carbon atom, as depicted in Figure 5a. And, the increase of atomic layers results in more polarization electrons in Pt_2/Gr (0.28 e in Figure S4) than in Pt_1/Gr (0.04 e). This would reduce the electric fields on the up-layered Pt-tip (Figure 1d and Figure 5d) and increase electrostatic repulsion between the negatively charged adsorbates and active Pt site.

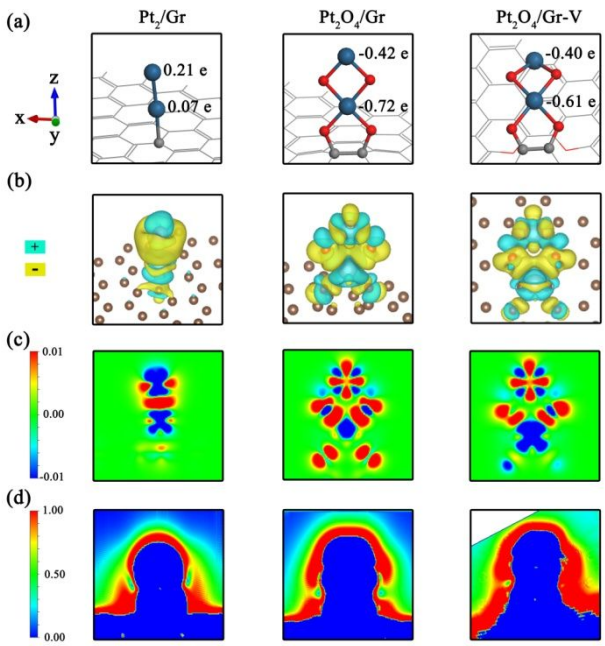

Figure 5. The binding structures and their corresponding electronic structures of the Pt_2/Gr, Pt_2O_4/Gr and Pt_2O_4/Gr-V catalysts. (a) Binding structures and DDEC charges of the Pt atoms; (b) 3D differential charge density maps; (c) 2D differential charge density maps; (d) 2D electric field maps. See Figure 1 for color coding.

The four-layered Pt_2O_4 on graphene can gain more polarization electrons (0.52 e in Figure S4) than the two-layered Pt_1O_2 (0.37 e). Comparing the charge transferring in Pt_1O_2/Gr and Pt_2O_4/Gr, we note that because O atoms have high electronegativity and low electrical conductivity, the polarization electrons collected by the Pt_2O_4 sharp-tip are mainly located on O atoms (Figure S4). The active up-layered Pt-tip is still positively charged (-0.42 e). Thus, compared to Pt_2/Gr, the electric field on the up-layered Pt-tip in Pt_2O_4/Gr is much stronger (Figure 5d), which can significantly promote the adsorption of O_2. As listed in Table 1, due to the enhanced binding stability of O_2, the CO poisoning rate $\boldsymbol{\Gamma_o}$ on Pt_2O_4/Gr has been reduced from 1.58 eV (Pt_2/Gr) to 0.59

eV, suggesting lower CO poisoning effect on Pt_2O_4/Gr. Different adsorption structural stabilities of O_2 further lead to different reaction activities. Figure 6 shows that the O_2 activation barrier on Pt_2O_4/Gr (1.31 eV) is 0.30 eV lower than that on Pt_2/Gr (1.61 eV). It should be emphasized that because the absolute value of O_2 adsorption (1.37 eV) on Pt_2/Gr (Figure S12) is lower than the energy barrier (1.61 eV), the O_2 molecules will be more inclined to be desorbed rather than disassociated on the pure Pt site.

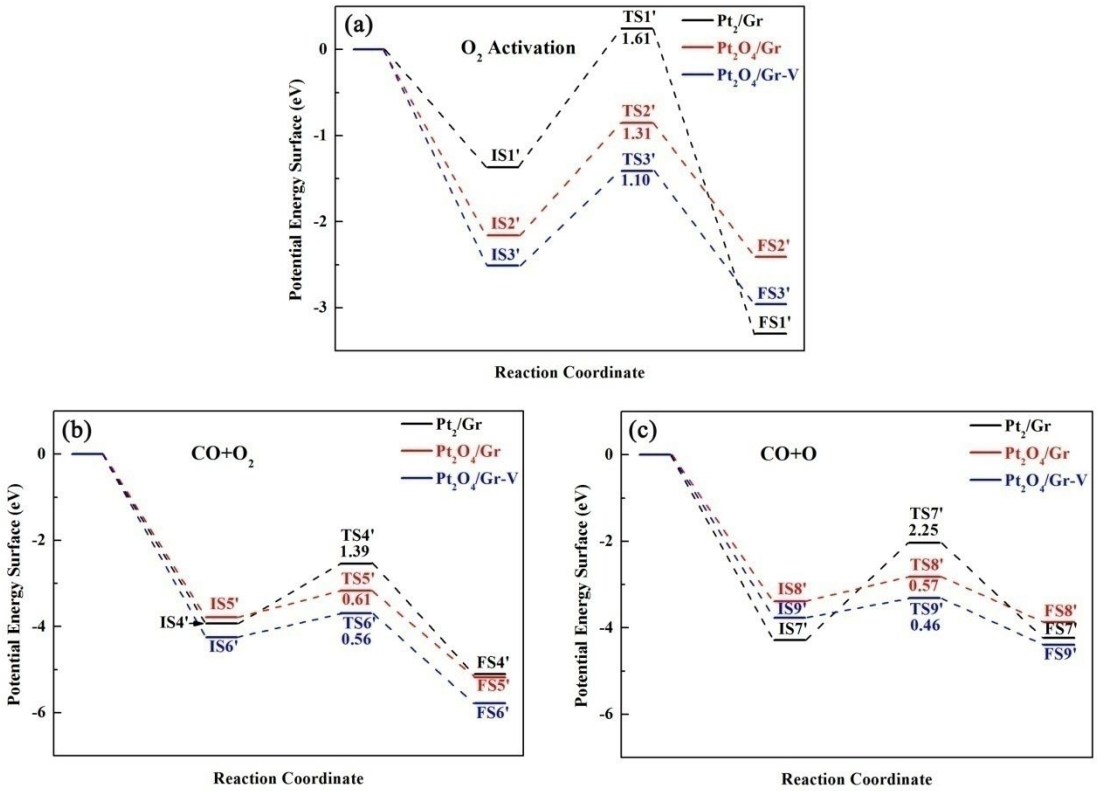

Figure 6. Potential energy diagrams for O_2 activation and CO oxidation (including the $CO+O_2$ and CO+O steps) on the Pt_2/Gr, Pt_2O_4/Gr and Pt_2O_4/Gr-V catalysts. The total energies of the bare surface and free adsorbate molecules are set to 0 eV. The optimized structures (including the transition states) and their binding energies are shown in Figures S12-S14.

In sharp contrast to Pt_2O_4/Gr, CO oxidation can hardly be catalyzed by Pt_2/Gr. It is shown in Figure 6b and 6c that although the co-adsorbed CO and O_2/O configuration on Pt_2/Gr are more stable than that on Pt_2O_4/Gr, the reaction barriers are much higher than those of the latter. Since the up-layered Pt atom in Pt_2/Gr holds subtle steric hindrance (comparing to Pt_1/Gr) and no repulsive force from the interfacial O atoms (compared to Pt_2O_4/Gr), the CO and O_2 can be adsorbed on two sides of the active Pt sites (Figure S13,). This special structure can enhance the stability of the binding state. However, due to the long distance between the C (in CO) and O (in O_2) atoms, the transition state (**TS4'**) on Pt_2/Gr cannot generate a metal-stable four-center structure (O-O-CO). Thus, the synergistic effect between the co-adsorbed CO and O_2 on Pt_2/Gr is not active, causing a high reaction energy barrier of 1.39 eV. Similar to the co-adsorbed CO and O_2 configuration, the weak steric hindrance effect and repulsive force on Pt_2/Gr result in a two-sides binding structure of CO+O (Figure S14). Furthermore, the CO is adsorbed by two Pt atoms. This means that when CO and O react to form CO_2, they need to break one more Pt-O bond, which greatly increases the energy barrier and thereby prohibits the second reaction step of "CO + O → CO" on Pt_2/Gr.

To gain a comprehensive understanding of the height of Pt tip on raised graphene-support, a detailed comparison study between Pt_1O_2/Gr and Pt_2O_4/Gr was carried out. As listed in Table 2 and 3, the adsorbates molecules gain fewer electrons from Pt_2O_4/Gr than those on Pt_1O_2/Gr. Moreover, the electronic structures in Figure 1 and 5 suggest that electric fields around the Pt-tip in Pt_2O_4/Gr are more decentralized than those in

Pt_1O_2/Gr, which is unfavorable for the adsorption of negatively charged adsorbates. The d-orbital center of the Pt-tip in Pt_2O_4/Gr (Figure 4) has a slight down-shift to lower energy in comparing with that of Pt_1O_2/Gr (from -2.43 eV to -2.53 eV). These three responses caused by the increase of the atomic layers actually weaken the stability of the adsorbate-catalyst configuration and reduce the activity of graphene-supported Pt catalyst (Figure 2 and 6).

3.4 O_2 Activation and CO Oxidation by Oxidized Pt_2 on Defective Graphene Surface.

To gain insight into the impact of the cluster atomic layers on the carbon-tip enhancement effect, Pt_2O_4 supported by a defective graphene oxide with one carbon vacancy was studied. In a similar manner to Pt_1O_2/Gr-V, after trying two possible anchoring scenarios, the energetically favorable Ortho-positioned Pt_2O_4 anchoring on Gr-V is chosen for further studies (Figure S15). For Pt_2O_4 supported on Gr-V, the height of carbon-tip is 1.54 Å (Figure 3), which is only 0.80 Å in Pt_2O_4/Gr. Comparing the charge transferring in Pt_2O_4/Gr and Pt_2O_4/Gr-V, one can see that the increase of the height of carbon-tip can promote the electron transferring between cluster and support (from 0.52 e in Pt_2O_4/Gr to 0.59 e in Pt_2O_4/Gr-V), and make the up-layered Pt-tip become less positively charged (from -0.42 e to -0.40 e in Figure S4).

The differential charge analysis in Table 3 indicates that the electron donation of the up-layered Pt-tip was improved by increasing the height of carbon-tip on Pt_2O_4/Gr-V.

As a result, the adsorbates can gain more electrons from Pt_2O_4/Gr-V than Pt_2O_4/Gr. The 2D electric field maps in Figure 5 exhibit the concentrated electric field of the up-layered Pt-tip atom in Pt_2O_4/Gr-V. In addition, the d-orbital center of the up-layered Pt-tip atom in Pt_2O_4/Gr-V is up-shifted to Fermi level (from -2.53 eV in Pt_2O_4/Gr to -1.60 eV). These thus enhance the stabilities of the adsorbate-catalyst configurations. While it is worth to mention that the electron transferring (Table 2 and 3), the localization of electric field (Figure 1d and 5d), and the up-shift of d-orbital center (Figure 4) of the up-layered Pt-tip atom in Pt_2O_4/Gr-V are actually weaker than those of Pt_1 atom in Pt_1O_2/Gr-V.

Table 3. The charge difference (before and after adsorption) of the active Pt sites **(Pt)** and the adsorbates **(ad)** on the Pt_2O_4/Gr and Pt_2O_4/Gr-V catalysts. $\Delta q = q_{aft} - q_{bef}$

	$\Delta q(O_2)$ (e)	$\Delta q(CO+O_2)$ (e)	$\Delta q(CO+O)$ (e)
Pt_2O_4/Gr(Pt)	-0.12	-0.03	-0.22
Pt_2O_4/Gr(ad)	0.27	0.17	0.27
Pt_2O_4/Gr-V(Pt)	-0.13	-0.06	-0.23
Pt_2O_4/Gr-	0.31	0.24	0.33

For O_2 activation and CO oxidation, as expected, both of the high carbon-tips on Pt_1O_2/Gr-V and Pt_2O_4/Gr-V can enhance the stability of the adsorbate-catalyst configurations (including O_2, $CO+O_2$ and CO+O). However, as the atomic layer of the oxidized Pt cluster increased, the enhancing effect (ΔE) is reduced, as listed in Table 4.

The enhanced stabilities of the adsorbates can promote the activities. Interestingly, a good linear relationship between the binding energy of adsorbates and energy barrier for the same catalytic process on various oxidized Pt sites on Gr is found in Figure 7. The chemisorption energies and their corresponding activities of O_2, CO+O_2 and CO+O all follow the order: Pt_1O_2/Gr-V > Pt_2O_4/Gr-V > Pt_1O_2/Gr > Pt_2O_4/Gr. This phenomenon further confirms our previous conclusion that for similar structured binding states, the binding energy of adsorbates will be a good descriptor to estimate the activity of different catalysts.[49] In combination with the lower CO poisoning effect (Γ_o follow the order: Pt_1O_2/Gr > Pt_2O_4/Gr > Pt_2O_4/Gr-V > Pt_1O_2/Gr-V), the Pt_1O_2/Gr-V would be a very promising catalyst for O_2 activation and CO oxidation , and some other related reactions.

Table 4. Calculated binding energies (E_b) and energy difference (ΔE) of O_2, CO+O_2 and CO+O on different Pt sites. $\Delta E = E_b(Pt_xO_{2x}/Gr) - E_b(Pt_xO_{2x}/Gr\text{-}V)$

	Pt_1O_2/Gr	Pt_1O_2/Gr-V	ΔE	Pt_2O_4/Gr	Pt_2O_4/Gr-V	ΔE
$E_b(O_2)$/eV	-2.42	-2.93	**0.51**	-2.16	-2.51	**0.35**
$E_b(CO+O_2)$/eV	-4.15	-4.70	**0.55**	-3.78	-4.25	**0.47**

E_b**(CO+O)/eV**	-3.70	-4.20	**0.50**	-3.39	-3.77	**0.38**

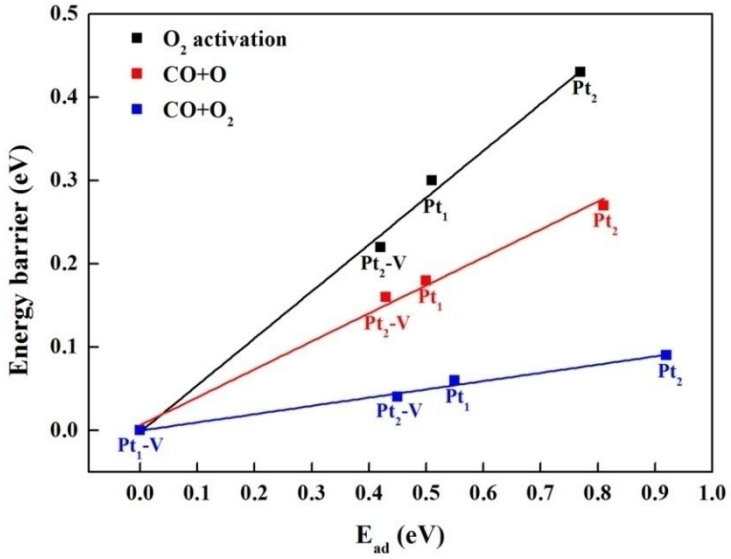

Figure 7. Correlations for the relative adsorption energies and energy barriers of the O_2 activation and CO oxidation (including the "CO+O_2" and "CO+O" steps) processes on the Pt-tip sites. The adsorption energy and energy barrier of the most favorable catalyst are both set to 0 eV. Here, the **Pt_1**, **Pt_2**, **Pt_1-V** and **Pt_2-V** represent the Pt_1O_2/Gr, Pt_2O_4/Gr, Pt_1O_2/Gr-V and Pt_2O_4/Gr-V catalysts, respectively.

4. CONCLUSIONS

This work represents one of the first attempts to obtain a comprehensive understanding of the sharp-tip enhancement effect of atomically dispersed Pt_1/Pt_2 catalysts on graphene supports. The simulation results demonstrate that the raised carbon-tip on the graphene oxide support with a carbon vacancy carries the following functions: (i) It facilitates electron transfer between the cluster and the support,

improving electron donation to the Pt-tip (active site); (ii) It enhances localization of the electric field on the Pt-tip; (iii) It up-shifts the d-orbital center of the Pt-tip atom toward the Fermi level. These responses can strengthen the interactions between the adsorbates and the catalysts. Detailed comparisons between the Pt_1O_2 and Pt_2O_4 clusters on Gr/Gr-V indicate that the enhancement effect of the carbon-tip is a long-range effect, and that it is reduced in the presence of oxidized atomic layers below the Pt-tip. The O_2 and CO adsorption capacities of the catalysts follow the order: Pt_1O_2/Gr-V > Pt_2O_4/Gr-V > Pt_1O_2/Gr > Pt_2O_4/Gr. In view of the linear relationship between the binding energy of adsorbates and the energy barrier for various Pt-tip sites on the raised graphene oxide platform, there activity follows the same order. Promoted by the carbon-tip enhancement effect, the energy barrier of the CO oxidation on Pt_1O_2/Gr-V has been reduced from 1.19 eV to 0.56 eV compared with Pt_1 on planar Gr, and the CO poisoning rate $\boldsymbol{\Gamma_o}$ has been reduced from 2.00 eV to 0.52 eV. Finally, combining the high catalytic activity and low CO poisoning effect, the Pt_1O_2/Gr-V catalyst should be the best catalyst for the O_2 activation and the CO oxidation. These findings provide important insights into the sharp-tip enhancement effect, leading to new strategies for development of efficient atomically dispersed transition metal catalysts.

Supporting Information Available: Calculation details for the ratio between the coverage of CO and O_2, and additional data presented in Figures S1-S12.

AUTHOR INFORMATION

Corresponding Author

* jiangj1@ustc.edu.cn. Phone: +86 551 63600029

ACKNOWLEDGMENTS

This work is supported by the National Key Research and Development Program of China (2018YFA0208603, 2017YFA0303500), National Natural Science Foundation of China (NSFC 21603042, 21633006, 21633007, 21703045, 21963007), DNL Cooperation Fund CAS (No. DNL201913), Natural Science Foundation of Guizhou Province ([2017]5790-01, [2020]1Y039). O.V.P. acknowledges support of the U.S. Department of Energy (Grant No. DE-SC0014429).

References

(1) L. Cao, et al., *Nature*, 2019, **565**, 631-635.

(2) J. Su, R. Ge, Y. Dong, F. Hao and L. Chen, *J. Mater. Chem. A*, 2018, **6**, 14025-14042.

(3) L. DeRita, S. Dai, K. Lopez-Zepeda, N. Pham, G. W. Graham, X. Pan and O. Christopher, *J. Am. Chem. Soc.*, 2017, **139**, 14150-14165.

(4) T. Kropp, Z. Lu, Z. Li, Y. H. C. Chin and M. Mavrikakis, *ACS Catal.*, 2019, **9**, 1595-1604.

(5) S. Song, Y. Wu, S. Ge, L. Wang, Y. Wang, Y. Guo, W. Zhan and Y. Guo, *ACS Catal.*, 2019, **9**, 6177-6187.

(6) P. Zhang, L. Liu, X. He, X. Liu, H. Wang, J. He and Y. Zhao, *J. Am. Chem. Soc.*, 2019, **141**, 6263-6270.

(7) J. Liu, H. Zhang, M. Qiu, Z. Peng, M. K. H. Leung, W. F. Lin and J. Xuan, *J. Mater. Chem. A*, 2020, **8**, 2222-2245.

(8) X. Zhao, X. Liu, B. Huang, P. Wang and Y. Pei, *J. Mater. Chem. A*, 2019, **7**, 24583-24593.

(9) M. Wang, C. Ye, H. Liu, M. Xu and S. Bao, *Angew. Chem., Int. Ed.*, 2018, **57**, 1963-1967.

(10) J. Liu, F. R. Lucci, M. Yang, S. Lee, M. D. Marcinkowski, A. J. Therrien, C. T. Williams and E. C. H. Sykes, *J. Am. Chem. Soc.*, 2016, **138**, 6396-6399.

(11) B. Zhang, G. Sun, S. Ding, H. Asakura, J. Zhang, P. Sautet and N. Yan, *J. Am. Chem. Soc.*, 2019, **141**, 8185-8197.

(12) Z. W. Chen, L. X. Chen, C. C. Yang and Q. Jiang, *J. Mater. Chem. A*, 2019, **7**, 3492-3515.

(13) N. J. O'Connor, A. S. M. Jonayat, M. J. Janik and T. P. Senftle, *Nat. Catal.*, 2018, **1**, 531-539.

(14) S. C. Ammal and A. Heyden, *ACS Catal.*, 2019, **9**, 7721-7740.

(15) H. Yan, C. Su, J. He and W. Chen, *J. Mater. Chem. A*, 2018, **6**, 8793-8814.

(16) F. Huang, et al., *J. Am. Chem. Soc.*, 2018, **140**, 13142-13146.

(17) C. Tang, B. Wang, H. Wang and Q. Zhang, *Adv. Mater.*, 2017, **29**, 1703185.

(18) Y. Li, Q. Zhang, C. Li, H. N. Fan, W. B. Luo, H. K. Liu and S. X. Dou, *J. Mater. Chem. A*, 2019, **7**, 22242-22247.

(19) W. Ren, X. Tan, W. Yang, W.; C. Jia, S. Xu, K. Wang, S. C. Smith and C. Zhao, *Angew. Chem., Int. Ed.*, 2019, **58**, 6972-6976.

(20) X. Cui, et al., *Angew. Chem., Int. Ed.*, 2016, **55**, 6708-6712.

(21) L. Zhang, et al., *Chem*, 2018, **4**, 285-297.

(22) D. Liu, et al., *Nat. Energy*, 2019, **4***,* 512-518.

(23) H. Jiang, Z. Hou and Y. Luo, *Angew. Chem., Int. Ed.*, 2017, **56**, 15617-15621.

(24) H. Yan, et al., *Nat. Commun.*, 2017, **8**, 1070.

(25) S. Han and B. Mullins, *ACS Catal.*, 2018, **8**, 3641-3649.

(26) J. X. Liu, Y. Su, I. A. W. Filot and J. M. A. Hensen, *J. Am. Chem. Soc.*, 2018, **140**, 4580−4587.

(27) G. Kresse and J. Furthmüller, *Phys. Rev. B*, 1996, **54**, 11169–11186.

(28) J. P. Perdew, K. Burke and M. Ernzerhof, *Phys. Rev. Lett.*, 1996, **77**, 3865–3868.

(29) P. E. Blöchl, *Phys. Rev. B*, 1994, **50**, 17953–17979.

(30) G. Kresse and D. Jouber, *Phys. Rev. B*, 1999, **59**, 1758–1775.

(31) O. Bengone, M. Alouani, P. E. Blöchl and J. Hugel, *Phys. Rev. B*, 2000, **62**, 16392–16401.

(32) S. Grimme, *J. Comput. Chem.*, 2006, **27**, 1787−1799.

(33) I. Fampiou and A. Ramasubramaniam, *J. Phys. Chem. C*, 2015, **119**, 8703−8710.

(34) S. Liu and S. Huang, *Carbon*, 2017, **115**, 11-17.

(35) T. A. Manz and N. G. Limas, *RSC Adv.*, 2016, **6**, 47771-47801.

(36) N. G. Limas and T. A. Manz, *RSC Adv.*, 2016, **6**, 45727-45747.

(37) Y. Wang, et al., *Nat. Commun.*, 2019, **10**, 1506.

(38) W. Sun, et al., *Nat. Mater.*, 2019, **18**, 732-739.

(39) X. Wang, G. Zhang, Z. Wang, L. Yang, X. Li, J. Jiang and Y. Luo, *Carbon* 2019, **143**, 700-705.

(40) G. Mills, H. Jonsson and G. K. Schenter, *Surf. Sci.*, 1995, **324**, 305- 337.

(41) G. Henkelman, B. P. Uberuaga and H. Jónsson, *J. Chem. Phys.*, 2000, **113**, 9901-9904.

(42) P. J. Feibelman, *Surf. Sci.*, 1994, **313**, L801-L805.

(43) L. R. Murphy, T. L. Meek, A. L. Allred and L. C. Allen, *J. Phys. Chem. A*, 2000, **104**, 5867-5871.

(44) L. Wang, X. Li, L. Jiang, B. Yang, Q. Liu, H. Xu, W. Zheng and S. He, *Angew. Chem., Int. Ed.*, 2018, **57**, 3349-3353.

(45) S. Hu. W. Xiao, W. Yang, J. Yang, Y. Fang, J. Xiong, Z. Luo, H. Deng, Y. Guo, L. Zhang and J. Ding, *ACS Appl. Mater. Interfaces*, 2018, **10**, 17167-17174.

(46) J. Yang, et al., *ACS Catal.*, 2019, **9**, 9751-9763.

(47) Z. P. Liu and P. Hu, *J. Am. Chem. Soc.*, 2002, **124**, 14770-14779.

(48) J. Xiao and T. Frauenheim, *J. Phys. Chem. C*, 2013, **117**, 1804−1808.

(49) C. Jia, X. Wang, W. Zhong, Z. Wang, O. V. Prezhdo, Y. Luo, and J. Jiang, *ACS Appl. Mater. Interfaces*, 2019, **11**, 9629−9640.

Table of Contents Graphic

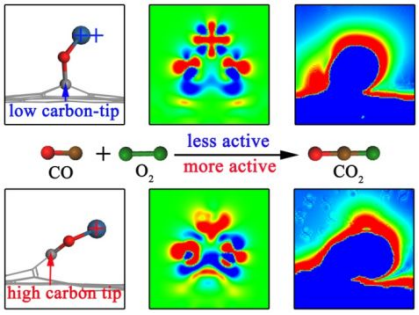

Sharp carbon-tip on defective graphene oxide induces strong local electric field on Pt-site, offering high catalytic performance.